Nonisothermal Crystallization and Multiple Melting Behaviors of β-Nucleated Impact-Resistant Polypropylene Copolymer

Xiaoxi Li, Haiyan Wu, Jingwei Chen, Jinghui Yang, Ting Huang, Nan Zhang, Yong Wang

Key Laboratory of Advanced Technologies of Materials (Ministry of Education), School of Materials Science & Engineering, Southwest Jiaotong University, Chengdu 610031, China

Received 30 September 2011; accepted 30 November 2011
DOI 10.1002/app.36633
Published online in Wiley Online Library (wileyonlinelibrary.com).

ABSTRACT: As a substitute of isotactic polypropylene in applications requiring excellent fracture resistance, impact-resistant polypropylene copolymer (IPC) has attracted much attention in recent years. In this study, a highly effective β-form nucleating agent (β-NA; an aryl amide compound) was introduced into IPC, and our attention was focused on the nonisothermal crystallization and subsequent melting behaviors of the nucleated samples. The nonisothermal crystallization behaviors were investigated on the basis of the different cooling rates and different concentrations of β-NA with differential scanning calorimetry, wide-angle X-ray diffraction (WAXD), and polarized optical microscopy. The results show that both the cooling rate and concentration of β-NA greatly determined the nonisothermal crystallization process and subsequent multiple melting behaviors. Further results show that the multiple melting behaviors were related to the transition in β crystallites and those between the β and α crystallites. The morphologies of the dispersed particles and the supermolecular structure of the matrix were characterized with scanning electron microscopy. Finally, the effect of the β-NA concentration on the fracture resistance of IPC was evaluated by measurement of the notched Izod impact strength. © 2012 Wiley Periodicals, Inc. J Appl Polym Sci 000: 000–000, 2012

Key words: crystallization; nucleation; poly(propylene) (PP)

INTRODUCTION

Impact-resistant polypropylene copolymer (IPC) is a novel polypropylene (PP) material exhibiting excellent fracture resistance. It is prepared through a two-step polymerization process. In the first stage, the bulk polymerization of propylene is induced by a special catalyst, $TiCl_4/MgCl_2$, and in the second stage, the copolymerization of propylene and ethylene is induced.[1–3] Therefore, the IPC material exhibits a complex multiphase structure consisting of PP homopolymer, an amorphous ethylene–propylene random copolymer (EPR), semicrystalline ethylene–propylene copolymers with different sequence lengths (E*b*Ps), and a few polyethylene (PE) homopolymers.[4–9] Morphological investigation has shown a multilayered core–shell structure of dispersed particles, with an inner core of PE, together with a part of PP, an intermediate layer of EPR, and an outer shell of E*b*P.[10,11] As a result, the E*b*P exhibits a role of compatibilizer to enhance the interfacial adhesion between the dispersed phase and the matrix; this endows the material with excellent fracture resistance.[12,13] Obviously, this is different from blends of immiscible PP and EPR by melt compounding, which have shown relatively poor fracture resistance because of their strong phase separation and low interfacial adhesion.[14,15]

The crystallization behavior of IPC has attracted much attention in recent years because of its complex multiphase structure. Feng and coworkers[10,16] introduced shear stress to the crystallization of IPC and found an amazing accelerated crystallization phenomenon. They believed that the external shear destroyed the multilayered core–shell structure by pulling out PE and the PE segments of E*b*P from the amorphous phase, and the PE segments aggregated together to form stable nuclei and played a key role in enhancing the subsequent crystallization rate of IPC. Through the fractionation of IPC and a subsequent solution-mixing process, Zheng and coworkers[17,18] proved the occurrence of cocrystallization between the PP chains in the E*b*P fraction and

Correspondence to: Y. Wang (yongwang1976@163.com).

Contract grant sponsor: National Natural Science Foundation of China; contract grant numbers: 51173151, 50973090.

Contract grant sponsor: Program for New Century Excellent Talents in University; contract grant number: NCET-08-0823.

Contract grant sponsor: Fundamental Research Funds for the Central Universities; contract grant numbers: SWJTU11CX142, SWJTU11ZT10.

in the PP homopolymer. Specifically, the molten-state annealing at relatively high temperature destroyed the core–shell structure and induced an increase in the size of the dispersed domains.[19] The overall crystallization rate and nucleation density decreased because of the variation of the nucleation ability of IPC induced by a coarsened microstructure and a decreased interface area.

Although it exhibits a complex multiphase structure, IPC's main component of is still the PP homopolymer. However, the presence of E*b*P strengthens the interfacial adhesion between the PP matrix and the dispersed core–shell particles. The occurrence of cocrystallization indicates that the E*b*P most likely influences the crystallization of the PP homopolymer to a certain extent. Therefore, in this work, we introduced a highly effective β-form nucleating agent (β-NA; an aryl amide compound with the trade name TMB-5) into IPC to further investigate the crystallization behavior of IPC. It has been proven that TMB-5 is a highly effective β-NA for the crystallization of isotactic PP, and the nucleation efficiency is comparable to values reported in the literature.[20–27] Similarly, both the nucleation efficiency of TMB-5 and the supermolecular structure of iPP are determined by the concentration of β-NA.[28–32] In fact, the crystallization and impact resistance of β-nucleated block copolymer PP have been investigated and reported in the literature,[33–36] but less attention has been focused on β-nucleated IPC, which exhibits a complex multiphase structure. The nonisothermal crystallization behavior and subsequent melting behaviors of nucleated IPC with different β-NA concentrations were investigated with differential scanning calorimetry (DSC), wide-angle X-ray diffraction (WAXD), and polarized optical microscopy (POM). The supermolecular structure and morphology of the nucleated IPC was characterized with scanning electron microscopy (SEM).

EXPERIMENTAL

Materials

All of the materials used in this study were commercially available. IPC [trade name SP179, melt flow rate = 6.2 g/10 min (190°C/2.16 kg)] was supplied by Lanzhou Petrochemical (Lanzhou, China). The ethylene content and rubber content were approximate 14.5 and 26.5 wt %, respectively. The β-NA aryl amide compound TMB-5 was kindly supplied by the Fine Chemicals Department of Shanxi Provincial Institute of Chemical Industry (Taiyuan, China).

Sample preparation

A master batch of IPC with 5 wt % β-NA was first prepared through the melt blending of IPC and TMB-5. Then, the master batch was diluted with IPC to obtain the corresponding compositions. The sample was designated SP/*x*TMB-5, where *x* represents the concentration of β-NA in the material. The melt blending of the compositions was conducted on a twin-screw extruder (TSE-20A, Nanjing Ruiya Polymer Processing Equipment Co., Ltd. Nanjing, China) with a screw speed of 200 rpm and temperatures of 150–170–190–200–210–210–200°C from the hopper to the die. After droplets were made, the pellets were injection-molded with an injection-molding machine (PS40E5ASE, Japan) with melt temperatures of 180–200–200–210°C from the hopper to the nozzle and a molding temperature of 25°C.

DSC

The nonisothermal crystallization and subsequent melting behaviors of the nucleated IPC samples were investigated with DSC (PerkinElmer Pyris-1, Fremont, USA). The instrument was calibrated with indium as a standard. A sample of about 5.0 mg was first quickly heated from room temperature to 200°C and maintained at this temperature for 5 min to erase the thermal history. Then, the sample was cooled down to room temperature at different cooling rates, that is, 5, 10, 20, and 40°C/min, and subsequently, the sample was heated again to 200°C at a heating rate of 10°C/min. All of the measurements were carried out in a nitrogen atmosphere.

WAXD

The crystalline structure of the sample obtained through the nonisothermal crystallization process was investigated with WAXD (Panalytical X'pert PRO diffractometer, Almelo, the Netherlands) with Ni-filtered Cu Kα radiation at 40 kV and 40 mA) in a continuous scanning angle range from 5 to 35°. The relative content of β-phase K_β value was calculated according to the following relation[37]:

$$K_\beta = I^\beta_{(300)} \Big/ \left[I^\beta_{(300)} + I^\alpha_{(110)} + I^\alpha_{(040)} + I^\alpha_{(130)} \right] \qquad (1)$$

where $I^\beta_{(300)}$ is the intensity of the diffraction of the (300) plane of β-PP and $I^\alpha_{(110)}$, $I^\alpha_{(040)}$, and $I^\alpha_{(130)}$ are the intensities of the diffractions of the (110), (040), and (130) planes of the α-PP, respectively.

POM

A POM instrument (Leica DMLP, So/ms, Germany) equipped with a hot stage (Linkman, Surrey, U.K.) was used to characterize the nonisothermal crystallization morphologies of the samples and record the subsequent morphological evolution during the heating process. First, the sample was heated to 200°C

and pressed into a slice with a thickness of about 20 μm. Then, the slice was transferred to the hot stage and maintained at 200°C for 5 min to erase the thermal history. Second, the sample was cooled down to room temperature at different cooling rates (5, 10, 20, and 40°C/min). The nonisothermal crystallization morphologies were imaged with a digital camera. Third, some representative samples were heated again to 200°C at a heating rate of 10°C/min, and the morphological evolution was also recorded.

SEM

The supermolecular structure of the injection-molded IPC matrix and the morphology of the dispersed phase were characterized with field emission SEM (FEI Inspect F, Portland, USA) at an accelerating voltage of 10 kV. Before SEM characterization, the injection-molded sample was fractured in liquid nitrogen perpendicularly to the flow direction. The cryofractured surface was first etched by *n*-heptane at 50°C for 3.5 h to remove the dispersed rubber phase. After it was washed very carefully, the cryofractured surface was further etched for 24 h with an etchant containing 1.3 wt % potassium permanganate ($KMnO_4$), 32.9 wt % concentrated sulfuric acid (H_2SO_4), and 65.8 wt % concentrated phosphoric acid (H_3PO_4) according to the methodology developed by Olley and Bassett.[38] Before SEM characterization, each of the samples was sputter-coated with a gold layer.

Impact measurement

The effect of β-NA on the fracture resistance of the nucleated IPC samples was evaluated through notched Izod impact measurement, which was conducted on a XC-22Z impact tester (Chengde Precision Testing Machine Company, Chengde, China) according to ASTM D 256-04. The impact measurement was carried out at 0°C, and the average values reported were derived from at least five specimens.

RESULTS AND DISCUSSION

Nonisothermal crystallization behaviors of the nucleated IPC samples

Figure 1 shows the DSC cooling curves of nucleated IPC samples obtained at different cooling rates. For comparison, the results of the nonnucleated IPC are also shown. As expected, for all of the samples, the crystallization peak temperature (T_{cp}) decreased with increasing cooling rate. To illustrate the effect of β-NA on the crystallization behavior of IPC, the DSC cooling curves of different samples obtained at a cooling rate of 10°C/min are shown in Figure 1(f). Obviously, the addition of β-NA induced an apparent variation in the crystallization behavior of IPC, and T_{cp} was proven to be greatly dependent on the β-NA concentration. For example, the nonnucleated IPC exhibited a T_{cp} of 115.9°C. At a β-NA concentration of 0.02 wt %, T_{cp} of IPC increased up to 122.5°C; this indicated a great heterogeneous nucleation effect of TMB-5 for IPC crystallization. A further increase in the concentration of β-NA induced a further increase in T_{cp}. The heterogeneous nucleation effect of β-NA for IPC crystallization was excellent at all cooling rates. Figure 2 shows the variation trend of T_{cp} as functions of the cooling rate and β-NA concentration. At all of the cooling rates applied in this work, it was proven that T_{cp} increased with increasing β-NA concentration. However, the nucleation efficiency of TMB-5 was more apparent at relatively lower β-NA concentrations, possibly because of the good dissolution and dispersion in the IPC matrix.[39] At higher β-NA concentrations, some particles of β-NA aggregated together and/or exhibited self-organization behavior; this led to a decrease in the nucleation efficiency of β-NA. As a result, only a slight increase in T_{cp} was observed.

Representative X-ray diffraction patterns of nonnucleated IPC and nucleated IPC samples after they were crystallized at different cooling rates are presented in Figure 3. The nonnucleated IPC samples were mainly characterized by α crystallites at 2θ values of 14.2, 16.8, and 18.5°, which corresponded to diffractions of the (110), (040), and (130) planes, respectively. This meant that the main crystalline structure in the nonisothermal crystallized IPC sample was α crystallites. Furthermore, at a cooling rate of 5°C/min, we observed a very weak diffraction peak at $2\theta = 16°$, which was attributed to the diffraction of the (300) plane of β crystallites. K_β was about 0.04. However, with an increase in the cooling rate, the intensity of the diffraction peak of the (300) crystal plane decreased gradually. Specifically, at a cooling rate of 40°C/min, the reflection of β-PP disappeared completely, and only the reflections of α crystallites were observed. Considering the complex multiphase structure of IPC with the presence of both EPR and E*b*P, we deduced that the formation of β crystallites was mainly due to the heterogeneous nucleation effect of dispersed particles. Similar results have been reported for blends of PP with other elastomers.[40,41] Furthermore, we noticed that the role of dispersed particles in IPC in inducting the formation of β crystallites was dependent on the cooling rate, namely, the duration of crystallization. Longer crystallization duration was favorable for the formation of β crystallites.

With the presence of β-NA, all of the nucleated IPC samples exhibited very strong diffraction peaks of β crystallites; this indicated the great nucleation effect of TMB-5 in inducing the formation of β crystallites in the IPC samples. K_β was calculated, and the results are shown in Figure 4. Apparently, the higher the concentration of β-NA was, the bigger K_β

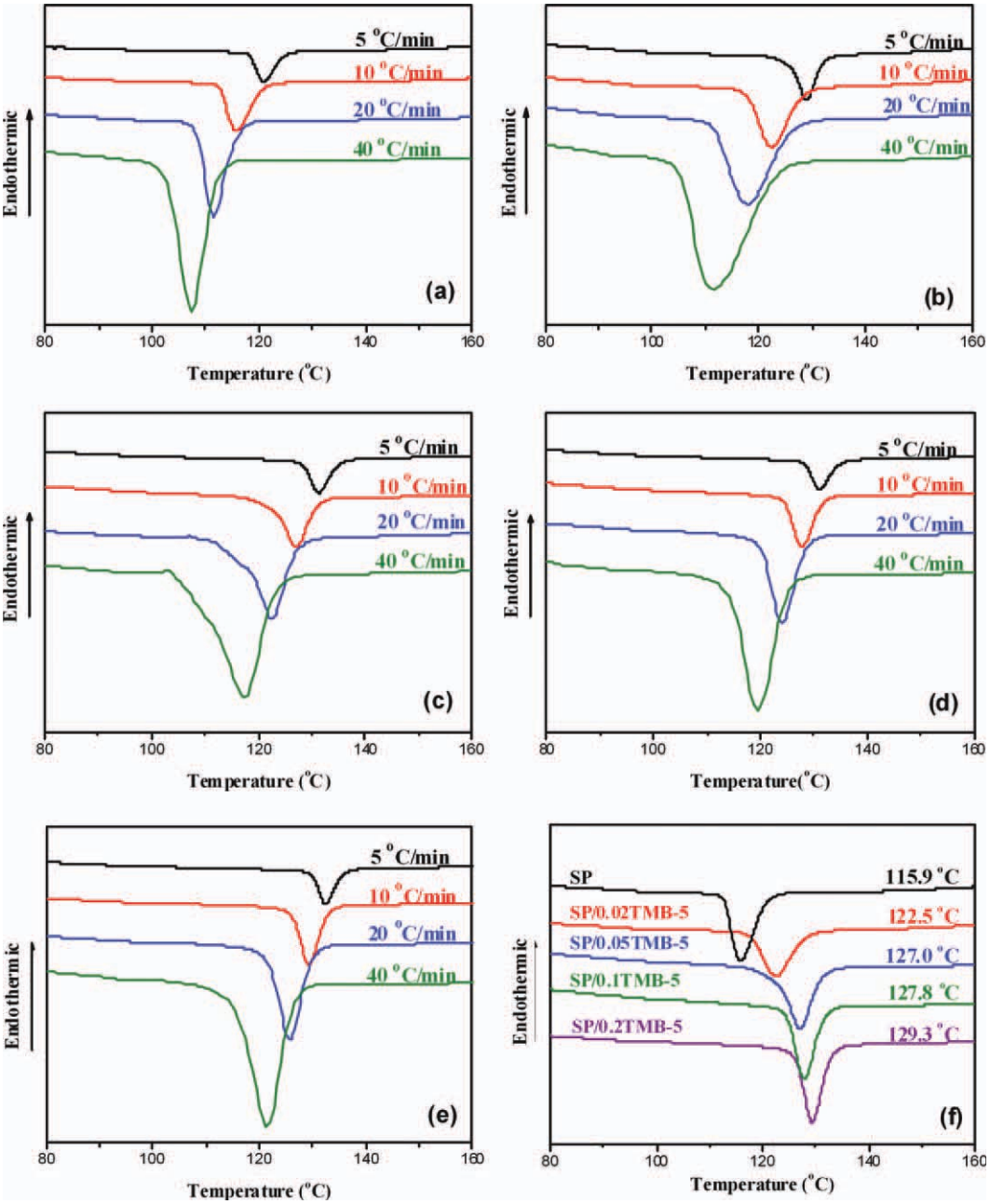

Figure 1 DSC cooling curves of IPCs nucleated by different concentrations of TMB-5 during nonisothermal crystallization at different cooling rates, as indicated in the graphs: (a) SP, (b) SP/0.02TMB-5, (c) SP/0.05TMB-5, (d) SP/0.1TMB-5, and (e) SP/0.2TMB-5. (f) Comparison of DSC cooling curves of different samples obtained at a cooling rate of 10°C/min. [Color figure can be viewed in the online issue, which is available at wileyonlinelibrary.com.]

was. Specifically, at relatively lower β-NA concentration (<0.1 wt %), specifically for the sample containing 0.02 wt % β-NA, K_β had a tendency to increase with an increase in the cooling rate. This was different from the phenomenon observed in the nonnucleated IPC samples and was also different from the observation of nucleated isotactic PP, in which the results show that the formation of β crystallites had a theoretical upper temperature of 140–141°C and a lower limit temperature of about 105°C.[42] Namely, the longer duration in this temperature range was favorable for the nucleation and growth of β crystallites and led to more β-crystallite formation. So far, it is still not clear why the nucleated IPC samples exhibited the different crystalline structures under the different cooling rates. However, we believe that the special dispersed particles in the IPC material were one of the possibilities. Similar to other immiscible elastomers used in PP blends, the dispersed particles mainly acted as the α-NA for the crystallization of isotactic PP, although they exhibited the nucleation role of inducing the

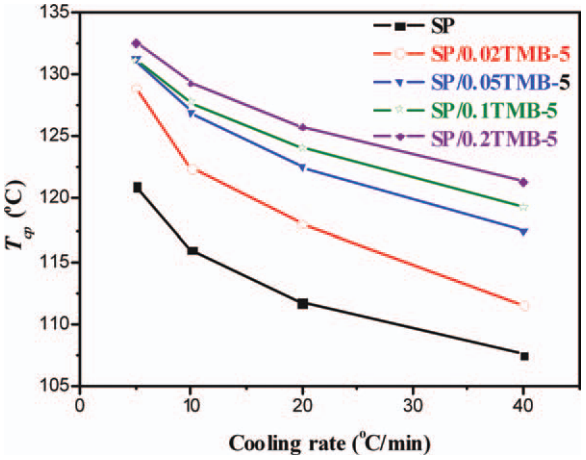

Figure 2 Variation of T_{cp} values of different samples as a function of the cooling rate. [Color figure can be viewed in the online issue, which is available at wileyonlinelibrary.com.]

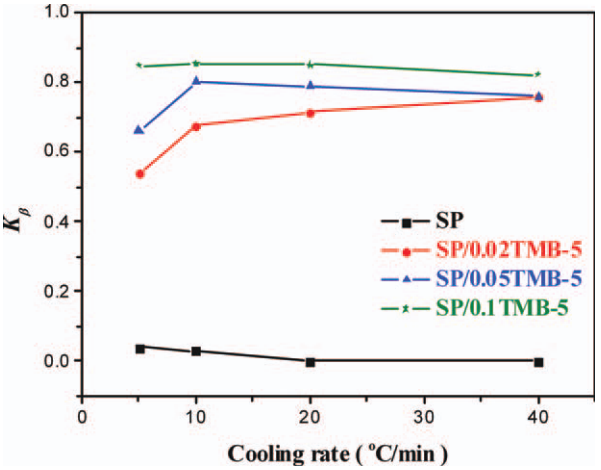

Figure 4 K_β values of different samples as a function of the cooling rate. [Color figure can be viewed in the online issue, which is available at wileyonlinelibrary.com.]

formation of β crystallites simultaneously. Therefore, in the nucleated IPC samples, there was competition between β-NA and the dispersed particles in inducing the crystallization of the PP homopolymer. Hence, we speculated that the competition depended on the cooling rate, that is, the duration of crystallization. Further work needs to be done to understand the real mechanism.

The evolution of the crystalline morphologies of the nonnucleated and nucleated IPC samples during

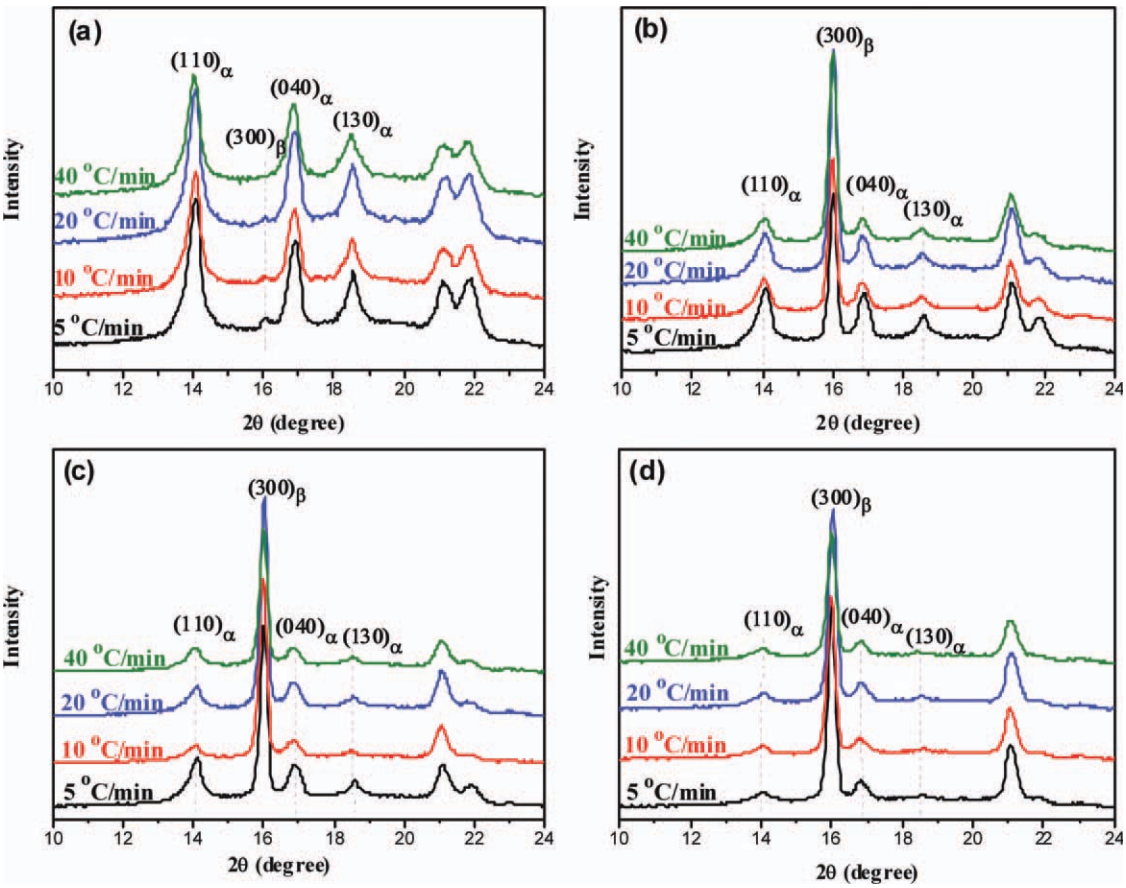

Figure 3 WAXD profiles of different samples after nonisothermal crystallization at different cooling rates, as indicated in the graphs: (a) SP, (b) SP/0.02TMB-5, (c) SP/0.05TMB-5, and (d) SP/0.1TMB-5. [Color figure can be viewed in the online issue, which is available at wileyonlinelibrary.com.]

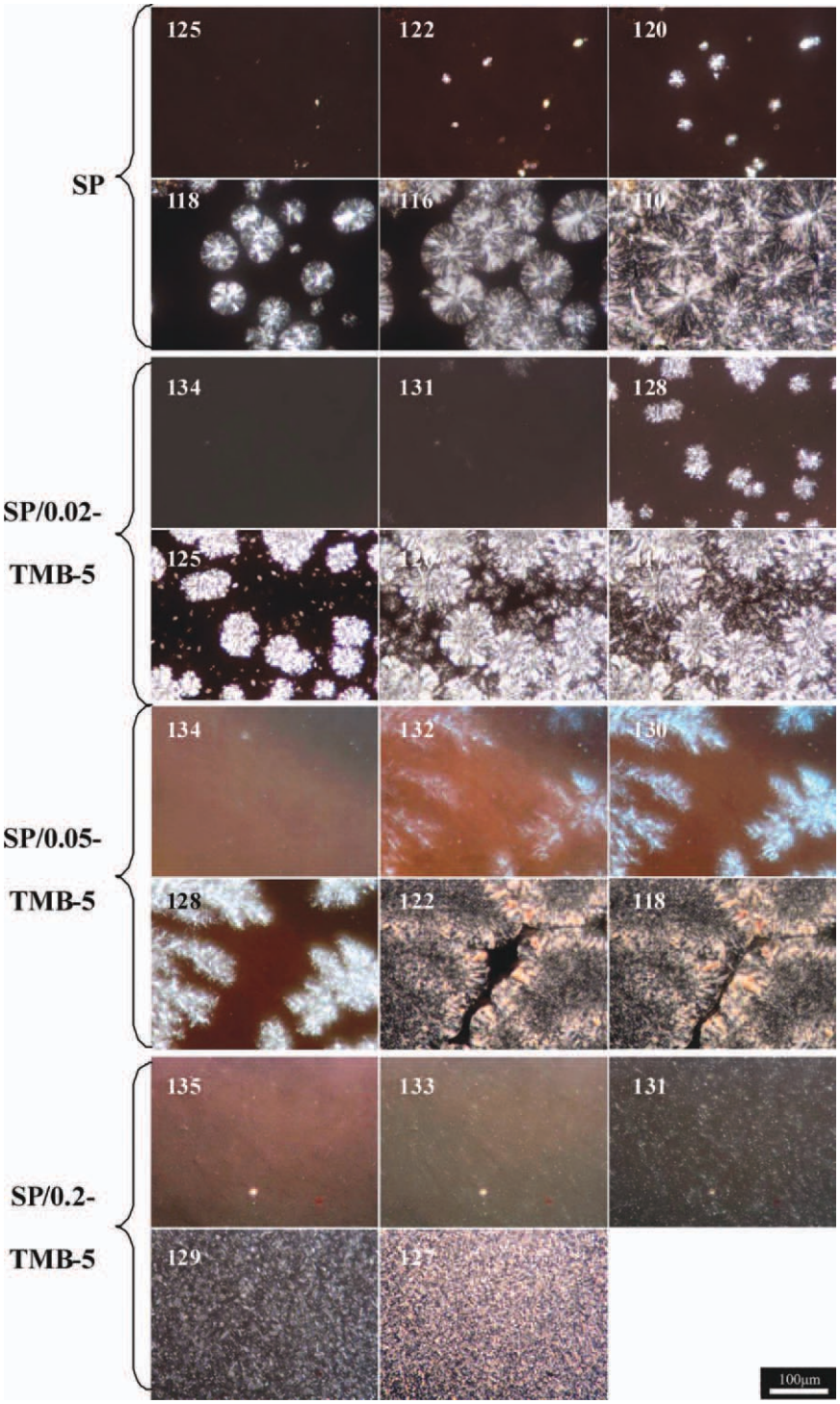

Figure 5 POM images showing the evolution of the crystalline morphologies of different samples during the nonisothermal crystallization process at a cooling rate of 5°C/min. The data shown in the images represent the real-time temperatures when the images were taken. [Color figure can be viewed in the online issue, which is available at wileyonlinelibrary.com.]

the nonisothermal crystallization process was characterized with POM. Herein, the representative results obtained at cooling rate of 5°C/min are shown in Figure 5. The data shown in these POM images are the real-time temperatures when the images were taken. As is well known, α spherulites present weak and positive birefringence because of their characteristic lamellar branching,[43–45] whereas β spherulites have a strong negative birefringence value. Thus, they are brighter and always appear to be brilliantly colored.[46–48] Therefore, from the POM images, one can roughly differentiate the presence of α or β spherulites. For the nonnucleated IPC sample, α spherulites with a typical Maltese cross were

observed. Because of the presence of dispersed particles with homogeneous distribution, which prevented lamellar growth in the front of the growth direction, the Maltese cross was very weak compared with that of isotactic PP as reported elsewhere. Specifically, the presence of E*b*P, which acted as the compatibilizer to intensify the interfacial adhesion between the PP homopolymer and the dispersed particles, also prevented the perfection of the α spherulites. Furthermore, after the completion of crystallization, although some tiny α-spherulites formed at relatively lower temperatures, many large α spherulites, with an average diameter of 100 μm, could be differentiated.

For the nucleated IPC samples, from Figure 5, one can see that the crystalline morphologies were greatly dependent on the concentration of β-NA. Complex crystallization behaviors were observed in SP/0.02TMB-5, including the heterogeneous nucleation of α and β spherulites. At a T_{cp} of 131°C, we observed the presence of β spherulites, and these β spherulites grew very fast. When T_{cp} was decreased to 125°C, in addition to the enlarged β spherulites, some sporadic α spherulites were also observed. Finally, SP/0.02TMB-5 exhibited α and β spherulites simultaneously. This agreed well with the observation from the WAXD measurements described previously. Because of the heterogeneous nucleation of β-NA, the presence of β spherulites occurred before that of the α spherulites. At the same time, part of the β-spherulite growth was changed to α-spherulite growth; this resulted in a novel crystalline morphology of the β spherulites (first formed), surrounded by a blend ring of β and α crystallites obtained at a lower T_{cp}. For SP/0.05TMB-5, we observed the formation of flowerlike β crystallites in the early stage of the crystallization process. With a decrease in T_{cp}, many small β crystallites were induced on the framework of the flowerlike β crystallites. The similar flowerlike morphology of β-PP has been reported elsewhere when isotactic PP was nucleated by a rare earth complex (WBG), and the reason given was the self-organization of WBG in the melt.[49] Thus, we suggest that TMB-5 self-organized into a flowerlike framework and then induced the heterogeneous nucleation of β crystallites. After the completion of the crystallization, it exhibited a similar crystalline morphology compared with SP/0.02TMB-5. With a further increase in concentration, TMB-5 preferred to agglomerate, and the flowerlike framework was destroyed. Because the self-organization process of TMB-5 could not catch the crystallization of the PP homopolymer up, only undissolved short fibrillar crystals, instead of self-organized long or dendritic fibers, served as nucleation sites. This resulted in the formation of tiny ambiguous β-crystallites. For other nonisothermal crystallization morphologies obtained at higher cooling rates (not shown here), the crystallization morphologies were similar to the ones observed at 5°C/min but with smaller size, increased crystal numbers, and more imperfect crystalline structures due to the faster crystallization process and the higher supercooling. Furthermore, the nucleated IPC samples exhibited a largely enhanced crystallization ability compared with the nonnucleated IPC sample. More visible crystallites were observed at relatively higher T_{cp} values, especially at a high concentration of β-NA.

Multiple melting behaviors of the nucleated IPC samples

Figure 6 shows the melting behaviors of the nonnucleated and nucleated IPC samples after the nonisothermal crystallization process. Figure 6(f) exhibits the effect of the β-NA concentration on the melting behaviors of different IPC samples that were obtained at cooling rate of 40°C/min. For the nonnucleated IPC samples, there were three endothermic peaks at 131.1, 148.8, and 162.7°C; these were attributed to the fusion of PE lamellae, β crystallites, and α crystallites, respectively. With an increase in the cooling rate, all of the endothermic peaks shifted to lower temperatures because of the formation of lamellae with smaller thickness at higher supercooling. When the cooling rate was higher than 20°C/min, it was very difficult to differentiate the fusion of β crystallites. This result agreed well with the observation obtained from WAXD measurements. Furthermore, a shoulder (shown as α_2 in the graph) was observed on the right side of the main endothermic peak (α_1) of the α crystallites, and the shoulder became more apparent at higher cooling rates. We believe that the reorganization process of α crystallites during the DSC heating process contributed to the presence of the shoulder.[50]

The nucleated IPC samples exhibited much more complex melting behaviors compared with the nonnucleated IPC sample. The first difference was that the endothermic peak of the PE lamellae could not be differentiated. This means that at least that the crystallization of PE was possibly inhibited by the presence of β-NA. Second, multiple melting behaviors accompanied by the recrystallization behaviors were observed for all of the nucleated IPC samples. For example, at a cooling rate of 5°C/min, SP/0.02TMB-5 exhibited three endothermic peaks at 152.0, 164.5, and 169.1°C (β_1, α_1', and α_2', respectively). With the increase in cooling rate, a new endothermic peak (β_2) at a relatively higher temperature was observed, and the intensity of the endothermic peak increased gradually. Simultaneously, the intensity of α_2' increased with increasing cooling rate. Furthermore, we observed the apparent

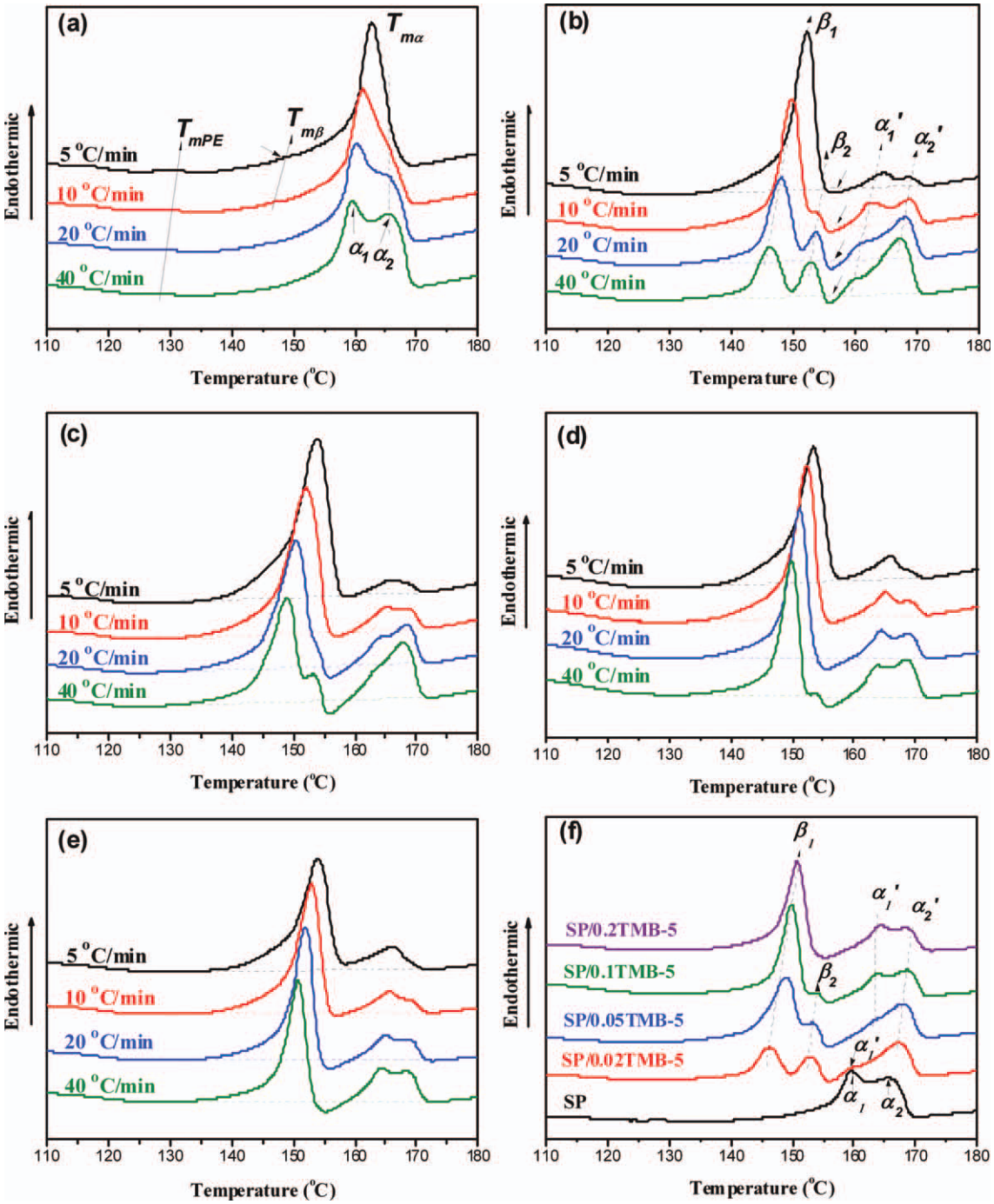

Figure 6 DSC heating curves of different samples after crystallization at different cooling rates, as indicated in the graphs: (a) SP, (b) SP/0.02TMB-5, (c) SP/0.05TMB-5, (d) SP/0.1TMB-5, and (e) SP/0.2TMB-5. (f) Comparison of the DSC heating curves of different samples after crystallization at a cooling rate of 40°C/min. T_{mPE} is the melting point of PE. [Color figure can be viewed in the online issue, which is available at wileyonlinelibrary.com.]

exothermic phenomenon during the DSC heating process (as shown by the solid arrows). This indicated the occurrence of the recrystallization process. It is well known that the β crystallite is a thermodynamically metastable phase. During the heating process, it has a tendency to melt first and then recrystallize as a stable α crystallite, and the latter melts further at relatively higher temperatures. Therefore, according to the previous description, one can imagine the different mechanisms for the multiple melting behaviors of nucleated IPC samples. Obviously, both β_1 and α_1' were due to the fusion of the original crystallites formed during the nonisothermal crystallization process. β_2 originated from the fusion of newly formed β crystallites during the DSC heating process through the transition of the

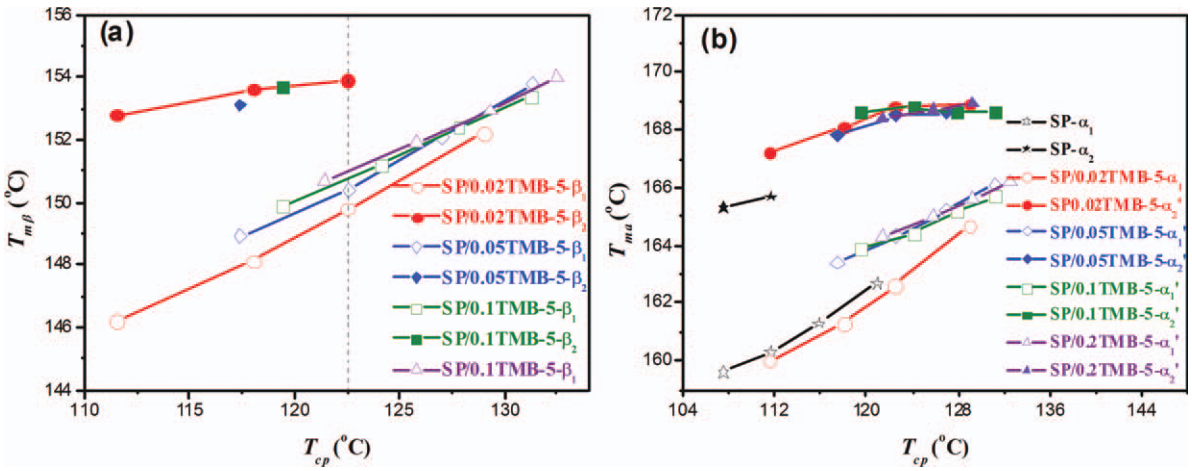

Figure 7 Dependence of (a) $T_{m\beta}$ and (b) $T_{m\alpha}$ on T_{cp}. [Color figure can be viewed in the online issue, which is available at wileyonlinelibrary.com.]

mesophase to β crystallites and/or the reorganization of original β crystallites with imperfect structures. α_2' was attributed to the fusion of newly formed α crystallites through the melt-recrystallization process of the β crystallites. The multiple melting behaviors became more and more remarkable with increasing cooling rate. With the increase of β-NA concentration, for example, when the samples were first crystallized at a cooling rate of 40°C/min [as shown in Fig. 6(f)], although the multiple melting behaviors were still apparent in the DSC heating curves, the intensity of β_2 weakened gradually and even disappeared completely at a β-NA concentration of 0.2 wt %. This meant that a higher concentration of β-NA was favorable for the formation of a β-lamellar structure with homogeneous distribution. The shift of β_1 to higher temperatures with increasing β-NA concentration was attributed to the lower supercooling during the nonisothermal crystallization process, which was favorable for the lamellar growth of β crystallites. Specifically, for SP/0.02TMB-5, the position of α_1' was similar to that of α_1. This indicated that both of them had the same growth mechanism, as proven by the previous description.

The values of melting temperature, including $T_{m\beta}$ and $T_{m\alpha}$ are melting points of β-phase and α-phase, respectively, were determined from the DSC heating curves, and their variation tendency as a function of T_{cp} are shown in Figure 7. The general trend was that a higher β-NA concentration facilitated an enhancement of $T_{m\beta}$. Similarly, $T_{m\beta}$ increased with increasing T_{cp}. Interestingly, it could be seen that when T_{cp} was higher than a critical value, only one endothermic peak (β_1) was achieved. Herein, the critical temperature was about 122.5°C. For $T_{m\alpha}$ of the α phase, at all T_{cp} values, the samples exhibited two values. The lower one (α_1') increased gradually with increasing T_{cp}, whereas α_2' changed slightly. This further indicated that α_1' was related to the α crystallites formed during the nonisothermal crystallization process, whereas α_2' to the newly formed α crystallites was achieved during the DSC heating process.

To further understand the multiple melting behaviors of nucleated IPC samples, the evolution of the crystalline morphologies during the heating process was recorded by *in situ* POM. Figure 8 shows the variation in the crystallization morphologies of the SP/0.05TMB-5 sample at a heating rate of 10°C/min. Before heating, the sample was crystallized at a cooling rate of 40°C/min. As described before, the nucleated sample exhibited a novel morphology resembling a so-called core–shell structure, with a core of β crystallites surrounded by a blend ring of β and α crystallites. The following analysis focuses on the evolution of such core–shell crystallization morphologies, which are marked by two concentric circles. When the temperature was increased up to 145°C [Fig. 8(b)], the shell became brighter; this indicated the perfection of β crystallites. This was possibly related to the transition of β_1 to β_2 and/or the transition of the mesophase to β crystallites. At 150°C [Fig. 8(c)], the shell was still bright, whereas the core became dim. This indicated the fusion of β_1. During heating from 150°C [Fig. 8(c)] to 153°C [Fig. 8(d)], newly formed α crystallites were observed. This indicated the transition of β_1 to α_2'. In the temperature range 153–157°C [Fig. 8(d–f)], the α crystallites dominated the whole sample. A further increase in the temperature led to the fusion of α crystallites. At 168°C [Fig. 8(h)], no apparent crystallites were observed; this indicated the complete melting of α crystallites. It should be pointed out that, with the limited distinguishability of the POM equipment, there was a slight difference between the temperatures relating to the fusion and transition of β crystallites indicated by the POM and DSC measurements.

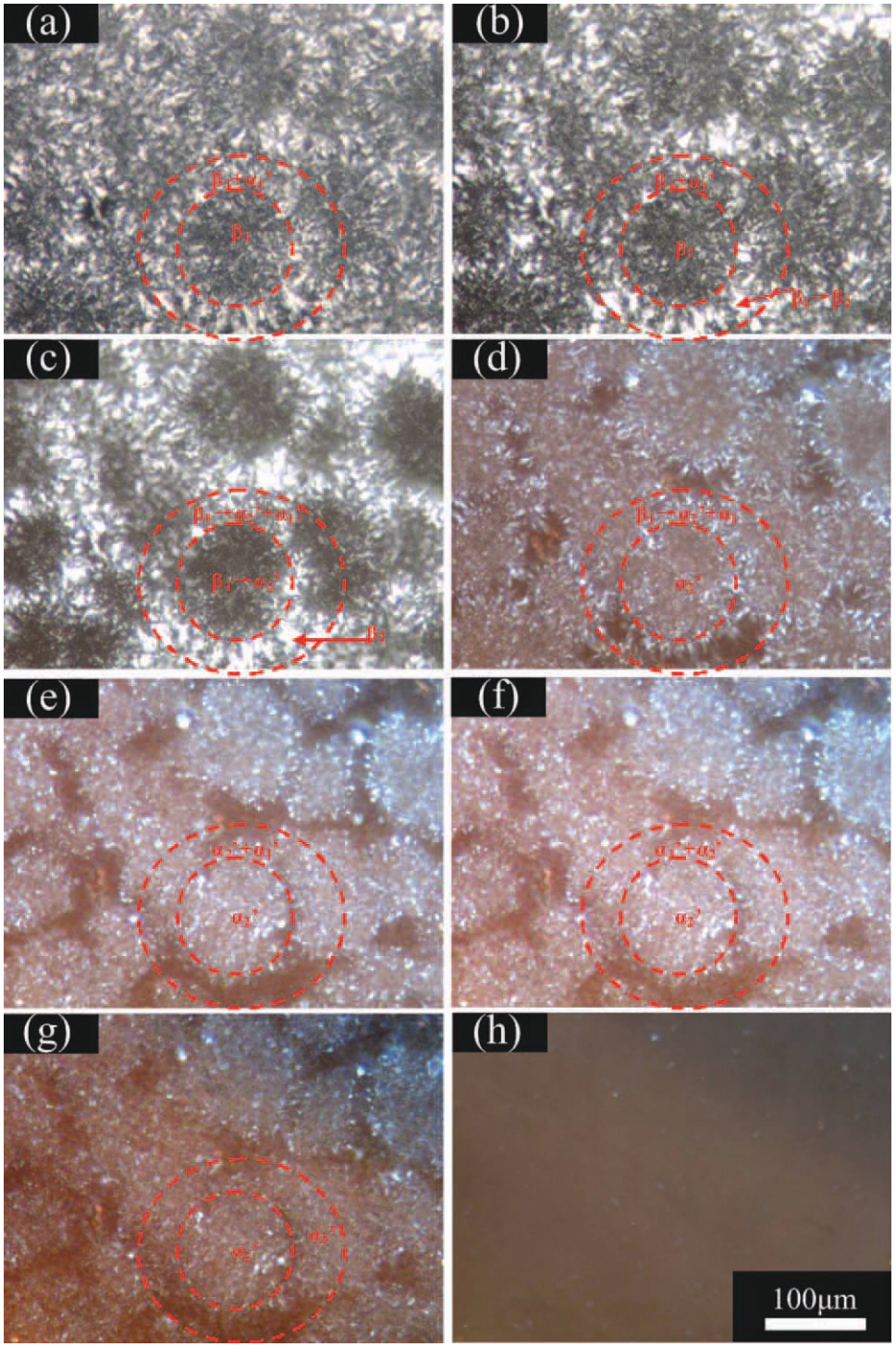

Figure 8 POM images of the crystalline morphologies of SP/0.05TMB-5 obtained at different temperatures during the melting process at a heating rate of 10°C/min: (a) 30, (b) 145, (c) 150, (d) 153, (e) 155, (f) 157, (g) 160, and (h) 168°C. The sample was first crystallized at a cooling rate of 40°C/min. [Color figure can be viewed in the online issue, which is available at wileyonlinelibrary.com.]

Supermolecular structure of the nucleated IPC samples

The supermolecular structures of the samples, with dispersed phases and molecular segments in the amorphous region being etched, were characterized by SEM, and the results are shown in Figure 9. For all of the samples, the dispersed particles with a core–shell structure exhibited a homogeneous distribution in the materials. The average diameter was about 0.96 μm. Obviously, the dark holes or the voids observed in the images represent the EPR

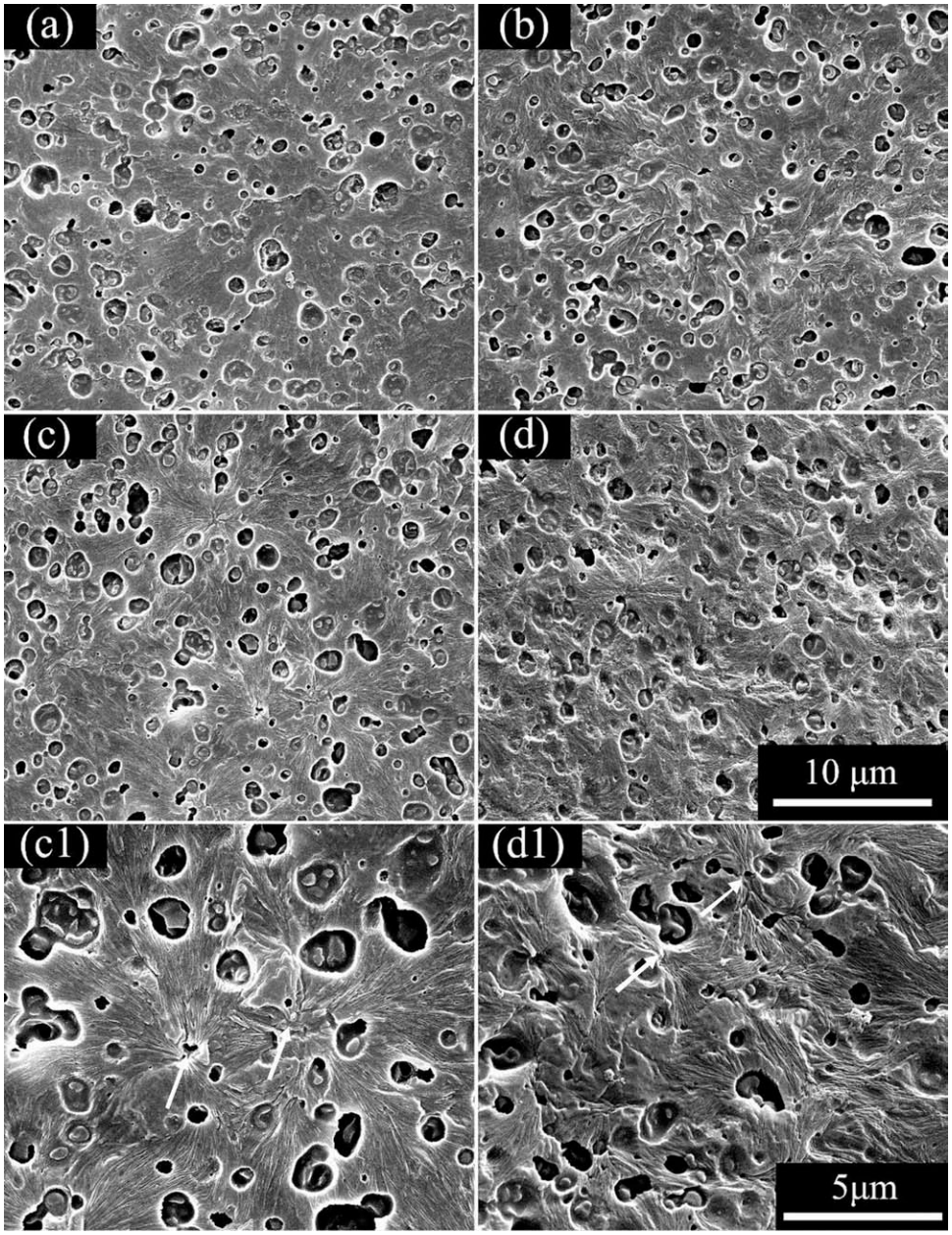

Figure 9 SEM images show the morphology of the dispersed particles and the supermolecular structures of the matrix: (a) SP, (b) SP/0.02TMB-5, (c) SP/0.05TMB-5, and (d) SP/0.1TMB-5. Morphologies of the (c1) SP/0.05TMB-5 and (d1) SP/0.1TMB-5 samples at higher magnifications.

part, which was removed by *n*-heptane, and the residual part in the center of the particles was ascribed to the region rich in PE segments.[13] The addition of β-NA did not influence the phase separation of IPC apparently, although the crystallization occurred at a relatively higher temperature. This further indicated that the phase separation and reconstruction of various components in IPC during the melt compounding and subsequent solidification occurred in a very short time.[12] Therefore, the mechanical properties of the nucleated IPC samples were mainly determined by the relative fraction and the supermolecular structure of β crystallites.

For the supermolecular structure of the matrix, the nonnucleated sample showed typical radial α spherulites with a large size of about 35 μm. With the presence of β-NA, typical β spherulites with a parallel lamellar structure were observed. Here, the β-NA was dissolved by strong acid, and the void, pointed out by arrows, showed the presence of β-NA in the materials. SP/0.02TMB-5 exhibited the coexistence of α/β spherulites [Fig. 9(b)]. This agreed well with the observations obtained from both the WAXD and DSC measurements. Unambiguous β spherulites with an average diameter of 20 μm were observed in the SP/0.05TMB-5 sample

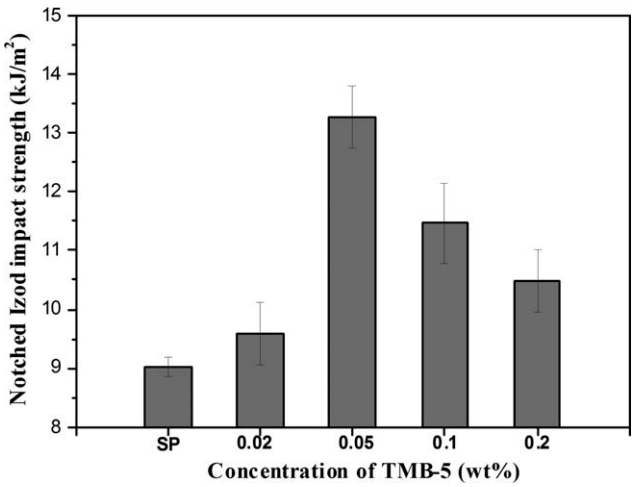

Figure 10 Variation of the notched Izod impact strength versus the concentration of TMB-5.

[Fig. 9(c)]. Particularly, flowerlike frameworks were visible at larger magnifications [Fig. 9(c1)]. As for SP/0.1TMB-5 [Fig. 9(d)], bundlelike β spherulites were discovered, and the average diameter was decreased to about 5 μm, which was measured along the length direction and was attributed to the largely increased nucleation density and agglomeration of β-NA, which prevented the growth of β spherulites.

Variation of the impact strength

The effect of the β-NA concentration on the fracture resistance was detected simply. As shown in Figure 10, the nonnucleated IPC sample exhibited a good impact strength (9.0 kJ/m^2) at a temperature of 0°C; this strength was much higher than that of the isotactic PP. The addition of β-NA induced a further enhancement in the impact strength due to the formation of large amounts of β crystallites. Similarly, the impact strength of the nucleated IPC samples was also dependent on the β-NA concentration. At relatively lower β-NA concentrations ($\leq$0.05 wt %), the impact strength increased gradually with increasing β-NA concentration and then up to the maximum value (13.3 kJ/m^2) at a β-NA concentration of 0.05 wt %. A further increase in the β-NA concentration led to a deterioration of the impact strength, but the values were still higher than that of the nonnucleated sample. The deterioration of impact strength was believed to be caused by the agglomeration of β-NA, which prevented the perfection of spherulites. For SP/0.05TMB-5, we suggest that the flowerlike morphology of the β crystallites, which intensified the adhesion among lamellae, was the main reason for the largely enhanced impact strength.[36]

CONCLUSIONS

In summary, a highly effective β-NA was introduced into IPC. The nonisothermal crystallization and subsequent melting behaviors of the nucleated samples were investigated in detail. The results show that both the concentration of β-NA and the cooling rate played great roles in determining the crystallization process and the crystalline morphologies of the nucleated IPC samples as well as the relative fraction of β crystallites. Specifically, some novel crystalline morphologies, including flowerlike and core–shell crystalline morphologies with β crystallites in the center and β/α crystallites in the outer ring, was observed in nucleated IPC samples with relatively lower β-NA concentrations. The nucleated IPC samples exhibited multiple melting behaviors during the heating process; these were related to the reorganization processes both in the β crystallites and between the β and α crystallites. Further results show that the multiple melting behaviors were greatly dependent on both the concentration of β-NA and the cooling rate applied during the nonisothermal crystallization process. SEM results show that the addition of β-NA did not influence the morphology of the dispersed particles. The impact measurement showed that the fracture resistance was further enhanced by β-NA, and there was a critical β-NA concentration (0.05 wt %) for enhancing the fracture resistance of the nucleated IPC samples.

References

1. Simonazzi, T.; Cecchin, G.; Mazzullo, S. Prog Polym Sci 1991, 16, 303.
2. Galli, P.; Haylock, J. C. Prog Polym Sci 1991, 16, 443.
3. Urdampilleta, I.; Gonzalez, A.; Iruin, J. J.; de la Cal, J. C.; Asua, J. M. Macromolecules 2005, 38, 2795.
4. Mirabella, F. M. Polymer 1993, 34, 1729.
5. Usami, T.; Gotoh, Y.; Umemoto, H.; Takayama, S. J Appl Polym Sci Appl Polym Symp 1993, 52, 145.
6. Xu, J.; Feng, L.; Yang, S.; Wu, Y.; Yang, Y.; Kong, X. Polymer 1997, 38, 4381.
7. Fan, Z. Q.; Zhang, Y. Q.; Xu, J. T.; Wang, H. T.; Feng, L. X. Polymer 2001, 42, 5559.
8. Cai, H. J.; Luo, X. L.; Ma, D. Z.; Wang, J. M.; Tan, H. S. J Appl Polym Sci 1999, 71, 103.
9. Horák, Z.; Fořt, V.; Hlavatá, D.; Lednický, F.; Večerka, F. Polymer 1996, 37, 65.
10. Song, S. J.; Feng, J. C.; Wu, P. Y.; Yang, Y. L. Macromolecules 2009, 42, 7067.
11. Zhang, C. H.; Shangguan, Y. G.; Chen, R. F.; Wu, Y. Z.; Chen, F.; Zheng, Q.; Hu, G. H. Polymer 2010, 51, 4969.
12. Chen, Y.; Chen, Y.; Chen, W.; Yang, D. C. Eur Polym J 2007, 43, 2999.
13. Chen, Y.; Chen, Y.; Chen, W.; Yang, D. C. J Appl Polym Sci 2008, 108, 2379.
14. Mehrdad, Y. P.; Raúl, Q.; Miguel, A.; López, M. Macromol Mater Eng 2003, 288, 875.
15. Yang, D. C.; Zhang, B. L.; Yang, Y. K.; Fang, Z.; Sun, G. F.; Feng, Z. L. Polym Eng Sci 1984, 24, 612.
16. Song, S. J.; Wu, P. Y.; Feng, J. C.; Ye, M. X.; Yang, Y. L. Polymer 2009, 50, 286.

17. Tan, H.; Li, L.; Chen, Z.; Song, Y.; Zheng, Q. Polymer 2005, 46, 3522.
18. Tan, H. S.; Xie, K.; Liu, W. H.; Hou, B.; Shangguan, Y. G.; Zheng, Q. Acta Polym Sinica 2006, 1, 1106.
19. Chen, R. F.; Shangguan, Y. G.; Zhang, C. H.; Chen, F.; Harkin-Jones, E.; Zheng, Q. Polymer 2011, 52, 2956.
20. Menyhárd, A.; Varga, J.; Molnár, G. J Therm Anal Calorim 2006, 83, 625.
21. Varga, J.; Menyhárd, A. Macromolecules 2007, 40, 2422.
22. Tang, J. G.; Wang, Y.; Liu, H. Y.; Belfiore, L. A. Polymer 2004, 45, 2081.
23. Blomenhofer, M.; Ganzleben, S.; Hanft, D.; Schmidt, H. W.; Kristiansen, M.; Smith, P.; Stoll, K.; Ma1der, D.; Hoffmann, K. Macromolecules 2005, 38, 3688.
24. Dou, Q. J Appl Polym Sci 2009, 111, 1738.
25. Lu, Q. L.; Dou, Q. e-Polymers 2008, no. 076.
26. Lu, Q. L.; Dou, Q. J Macromol Sci Phys 2008, 47, 463.
27. Lu, Q. L.; Dou, Q. J Polym Res 2009, 16, 555.
28. Dong, M.; Guo, Z. X.; Su, Z. Q.; Yu, J. J Polym Sci Part B: Polym Phys 2008, 46, 1183.
29. Dong, M.; Guo, Z. X.; Yu, J.; Su, Z. Q. J Polym Sci Part B: Polym Phys 2008, 46, 1725.
30. Dong, M.; Guo, Z. X.; Yu, J.; Su, Z. Q. J Polym Sci Part B: Polym Phys 2009, 47, 314.
31. Dong, M.; Guo, Z. X.; Su, Z. Q.; Yu, J. J Appl Polym Sci 2011, 119, 1374.
32. Bai, H. W.; Wang, Y.; Zhang, Z. J.; Han, L.; Li, Y. L.; Liu, L.; Zhou, Z. W.; Men, Y. F. Macromolecules 2009, 42, 6647.
33. Zhang, X.; Shi, G. Thermochim Acta 1994, 235, 49.
34. Zhang, X.; Shi, G. Polymer 1994, 35, 5067.
35. Varga, J.; Mudra, I.; Ehrenstein, G. W. J Appl Polym Sci 1999, 74, 2357.
36. Chen, H. B.; Karger-Kocsis, J.; Wu, J. S.; Varga, J. Polymer 2002, 43, 6505.
37. Turner-Jones, A.; Aizlewood, J. M.; Beckett, D. R. Makromol Chem 1964, 75, 134.
38. Olley, R. H.; Bassett, D. C. Polymer 1982, 23, 1707.
39. Varga, J.; Menyhárd, A. Macromolecules 2007, 40, 2422.
40. Li, X. X.; Wu, H. Y.; Han, L.; Huang, T.; Wang, Y.; Bai, H. W.; Zhou, Z. W. J Polym Sci Part B: Polym Phys 2010, 48, 2108.
41. Ying, J. R.; Liu, S. P.; Guo, F.; Zhou, X. P.; Xie, X. L. J Therm Anal Calorim 2008, 91, 723.
42. Varga, J. J Macromol Sci Phys 2002, 41, 1121.
43. Khoury, F. J. J Res Nat Bur Stand Sect A 1966, 70, 29.
44. Binsbergen, F. L.; De Lange, B. G. M. Polymer 1968, 9, 23.
45. Lotz, B.; Wittmann, J. C. J Polym Sci Part B: Polym Phys 1986, 24, 1541.
46. Padden, F. J.; Keith, H. D. J Appl Phys 1959, 30, 1479.
47. Norton, D. R.; Keller, A. Polymer 1985, 26, 704.
48. Varga, J. J Mater Sci 1992, 27, 2557.
49. Luo, F.; Geng, C. Z.; Wang, K.; Deng, H.; Chen, F.; Fu, Q.; Na, B. Macromolecules 2009, 42, 9325.
50. Wlochowicz, A.; Eder, M. Polymer 1984, 25, 1268.